Progress In Electromagnetics Research, Vol. 144, 103–114, 2014

Azimuth Stacking Algorithm for Synthetic Aperture Radar Imaging

Zhe Li[1, *], Tian Jin[2], Junjie Wu[3], Jian Wang[1], and Qing Huo Liu[4]

Abstract—The aim of this paper is to present a frequency domain method for synthetic aperture radar (SAR) imaging. By using two consecutive linear mappings along Doppler and frequency domains, an azimuth-dependent SAR transfer function has been discovered. Based on this new transfer function, the SAR image can be reconstructed by the proposed azimuth stacking algorithm. The new algorithm can form SAR image at each azimuth position without DFT wrap around errors. If Chirp z-transform (CZT) is applied to carry out the two consecutive mappings (since they are linear mappings), the proposed algorithm will not require interpolations and thus its reconstructed image would be free of truncation errors. The new algorithm has been validated using both simulated and experimental ultrawideband/widebeam (UWB/WB) SAR data.

1. INTRODUCTION

Intrinsically, the challenge of processing synthetic aperture radar (SAR) data comes from the fact that a long coherent aperture is needed to improve target's azimuth resolution. This mainly results in two opposite effects: 1) the desired longer illuminating time for each target in the imaged scene to improve azimuth resolution; and 2) the range dependent signal dispersion along azimuth direction in the two dimensional (2D) signal domain (range compression assumed). Due to the latter effect, namely the space-variance of SAR signal, SAR image formation is inherently a 2D processing [1]. How to properly correct and focus the space-variant dispersed signal on desired location is the main task of SAR signal processing. This can be coped with directly by the full 2D time domain correlation techniques. One representative of the time domain processing is the backprojection method [1–3], which can be very precise for all SAR configurations (even with motion errors), but are time-consuming and thus impractical for most of the SAR systems. In recent years, aiming to enhance its computational efficiency, several fast factorized backprojection methods have been proposed [4–7].

On the other hand, great efforts have been made to explore the efficiency of the frequency domain correlation techniques. By separating the signal's space-variant dispersion effect into range migration and azimuth dispersion parts, the Range-Doppler (RD) domain algorithms can form SAR image efficiently in two steps: bulk range cell migration correction (RCMC) and azimuth compression. The bulk RCMC can be implemented either by interpolation [8] or by the Chirp scaling (CS) technique [9, 10] in the RD domain for low squint case. To handle data of high squint mode SAR systems and/or the ultrawideband/widebeam (UWB/WB) SAR systems, several extended chirp scaling (ECS) algorithms [11–15] have been developed in the past years by incorporating different higher order terms of the Taylor series expansion on range frequency of the 2D SAR spectrum. The RD algorithms are very fast for only involving FFT and complex phase multiplications. However, besides the requirement of the Chirp modulated signal, they usually fail to properly focuse the UWB/WB SAR data, even with much higher order terms of the Taylor expansion considered [15]. Therefore, the accurate frequency domain

Received 22 November 2013, Accepted 31 December 2013, Scheduled 6 January 2014

* Corresponding author: Zhe Li (lizhee@gmail.com).

[1] Laboratory of Remote Sensing and Geospatial Science, Cold and Arid Regions Environmental and Engineering Research Institute, CAS, Lanzhou, Gansu 730000, China. [2] College of Electronic Science and Engineering, National University of Defense Technology, Changsha, Hunan 410073, China. [3] School of Electronic Engineering, University of Electronic Science and Technology of China, Chengdu, Sichuan 611731, China. [4] Department of Electrical and Computer Engineering, Duke University, Durham, NC 27708, USA.

method, like ω-k algorithm [16–18] and its extended version [19], are still competitive alternatives to SAR imaging.

The contribution of the work is to present a new frequency domain SAR imaging algorithm. The method is *Azimuth Stacking Algorithm (ASA)*. It first reshapes SAR 2D spectrum (or equivalent, SAR transfer function) by using two consecutive one-dimensional (1D) linear mappings along Doppler domain and frequency domain. Due to the mappings, the range-dependent SAR transfer function evolves into azimuth-dependent. Then, the targets at each azimuth position can be accurately reconstructed by the stacking approach [2]. Finally, the outcomes at each azimuth position can be combined to form a 2D SAR image. The new algorithm thus can form SAR image at each azimuth position without DFT wrap around errors. If Chirp z-transform (CZT) [20, 21] is applied to carry out the two consecutive mappings (since they are linear mappings), the proposed algorithm will not require interpolations and its reconstructed image would be free of truncation errors.

The rest of this paper is organized as follows: in Section 2, the proposed azimuth stacking algorithm will be mathematically derived and summarized. Section 3 describes how the azimuth stacking algorithm can be implemented via CZT, and a detailed algorithm will be presented. The main characteristics of the proposed algorithm is commented in Section 4. Section 5 gives both the simulation and the experimental results. Finally, Section 6 concludes the paper.

2. DERIVATION OF THE AZIMUTH STACKING ALGORITHM

In order to facilitate our analysis, we will use a simplified point scatterer/target response to describe the following derivations. This means that the radar radiation pattern and the limitations of different SAR modes (such as stripmap and spotlight modes) will not be included in our analysis. Because only phase information matters for focusing SAR signal, while the antenna radiation pattern and mode selection only affects the focusing pattern. Then, after asymptotically evaluating, the 2D SAR spectrum (range compressed) of a point scatterer located at (x, r) can be given as,

$$S(k_u, \omega) = \exp\left\{ -j\sqrt{(2k)^2 - k_u^2}\, r - jk_u x \right\}, \tag{1}$$

in which the insignificant slowly varying amplitude terms and constants are suppressed [15, 17]. Where, k_u is the wavenumber variable corresponding to the azimuth (antenna illuminating) position u; ω the angular velocity of the transmitted pulse, and $k \equiv \frac{\omega}{c}$ the corresponding wavenumber variable.

Based on the SAR 2D spectrum (1), the proposed azimuth stacking algorithm will be derived in this section. This mainly consists of three parts: Doppler domain mapping, frequency domain mapping, and azimuth stacking. The two consecutive mappings will change the conventional range-dependent SAR transfer function (or 2D spectrum) into azimuth-dependent.

2.1. Doppler Domain Mapping

Defining the mapping along Doppler domain,

$$k'_u = k_u \cdot \alpha(k), \tag{2}$$

where k'_u is the Doppler after mapping; $\alpha(k)$ is the frequency dependent linear mapping operator, defined as

$$\alpha(k) = \frac{k_c}{k}. \tag{3}$$

Then, after substituting (2) and (3) into (1) for k_u, the Doppler domain mapped SAR 2D spectrum can be obtained, after some rearrangement, as

$$S(\omega, k'_u) = \exp\left\{ -j2k \left[\sqrt{1 - \left(\frac{k'_u}{2k_c}\right)^2}\, r + \frac{k'_u}{2k_c}\, x \right] \right\}. \tag{4}$$

2.2. Frequency Domain Mapping

Defining the mapping along the frequency domain,

$$k_r = 2k \cdot \beta(k'_u), \tag{5}$$

where k_r is the frequency domain after the mapping; $\beta(k'_u)$ is the Doppler dependent linear mapping operator, defined as

$$\beta(k'_u) = \sqrt{1 - \left(\frac{k'_u}{2k_c}\right)^2}. \tag{6}$$

Then, by substituting (5) and (6) into (4), and after some rearrangement, the frequency domain mapped SAR 2D spectrum can be achieved as

$$S(k'_u, k_r) = \exp\left\{-jk_r\, r - jk_r \frac{k'_u}{\sqrt{4k_c^2 - {k'_u}^2}}\, x\right\}. \tag{7}$$

At this stage, it would be worthwhile to point out that after Doppler domain mapping and frequency domain mapping, the range-dependent SAR transfer function (1) has now been transformed into an azimuth-dependent SAR transfer function (7). This new transfer function enables SAR image to be reconstructed via the stacking method [2] along azimuth direction.

2.3. Azimuth Stacking Reconstruction Method

Mathematically, the SAR image can be obtained by performing a 2D inverse Fourier transform of the target spectrum $\Gamma(k_x, k_r)$

$$\gamma(x, r) = \int_{k_x}\int_{k_r} \Gamma(k_x, k_r) \exp\left\{jk_x x + jk_r r\right\} dk_x\, dk_r. \tag{8}$$

In order to map the above reconstruction from (k_x, k_r) domain into the SAR data domain (k'_u, k_r), see (7), we perform the following mapping

$$k_x = k_r \frac{k'_u}{\sqrt{4k_c^2 - {k'_u}^2}}, \tag{9}$$

Then,

$$\gamma(x, r) = \int_{k'_u}\int_{k_r} S(k'_u, k_r) J(k'_u, k_r) \exp\left\{jk_r \frac{k'_u}{\sqrt{4k_c^2 - {k'_u}^2}}\, x + \; jk_r r\right\} dk'_u\, dk_r, \tag{10}$$

where

$$J(k'_u, k_r) = k_r \frac{4k_c^2}{(4k_c^2 - k_u'^2)^{3/2}}, \tag{11}$$

is the Jacobian of the transform from (k_x, k_r) into (k'_u, k_r), which is a slowly-fluctuating amplitude function. Thus its contribution in the reconstruction is negligible and will be ignored in the following analysis.

Then, after some rearrangement of (10), we will have

$$\gamma(x, r) = \int_{k_r} jk_r r\, dk_r \int_{k'_u} S(k'_u, k_r) \exp\left\{jk_r \frac{k'_u}{\sqrt{4k_c^2 - {k'_u}^2}}\, x\right\} dk'_u. \tag{12}$$

Let

$$\phi(k'_u, k_r; x) = \exp\left\{jk_r \frac{k'_u}{\sqrt{4k_c^2 - {k'_u}^2}}\, x\right\}, \tag{13}$$

thus, the targets function $\gamma(x_i, r)$ at azimuth position x_i can be reconstructed by

$$\gamma(x_i, r) = \underbrace{\int_{k_r} jk_r r\, dk_r \quad \underbrace{\int_{k'_u} \underbrace{S(k'_u, k_r) \cdot \phi(k'_u, k_r; x_i)}_{\text{1) filtering}}\, dk'_u}_{\text{2) summation along Doppler domain}}}_{\text{3) 1D inverse Fourier transform along } k_r \text{ domain}} . \tag{14}$$

2.4. The Azimuth Stacking Algorithm

In summary, according to the above derivations, the proposed azimuth stacking algorithm (see Fig. 1) can then be given as below:

1) Range compression without IFFT;
2) Azimuth FFT to obtain SAR 2D spectrum;
3) Doppler domain mapping (2);
4) Frequency domain mapping (5);
5) Phase multiplication of $S(k'_u, k_r)$ by $\phi(k'_u, k_r; x_i)$; which corresponding to filtering the data for each azimuth position;
6) Integrating (summing) the multiplication result over the Doppler domain k'_u to give $\gamma(x_i, k_r)$;
7) Inverse Fourier transform of $\gamma(x_i, k_r)$ to generate the reflectivity image $\gamma(x_i, r)$ at azimuth position x_i.
8) Iterating step 4) to step 6) for all azimuth positions;
9) Combing $\gamma(x_i, r)$ along azimuth direction to yield 2D SAR image.

It should be noted that since the Doppler domain mapping and frequency domain mapping are linear mappings, they can be efficiently implemented by the Chirp z-transform (CZT) [20, 21] that without suffering from the interpolation truncation error.

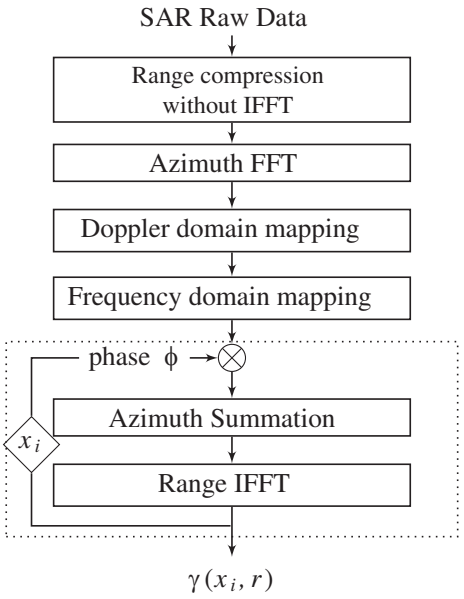

Figure 1. Block diagram of the proposed azimuth stacking algorithm. The highlighted part with dashed box denotes the azimuth stacking processing.

3. THE EFFICIENT IMPLEMENTATION OF THE AZIMUTH STACKING ALGORITHM

In this section, we will present a detailed algorithm to efficiently implement the proposed algorithm. The efficiency here means we will avoid any usage of interpolation to carry out the two mappings by CZT [20], which only need FFTs and phase multiplications. A block diagram of the azimuth stacking algorithm is shown in Fig. 2.

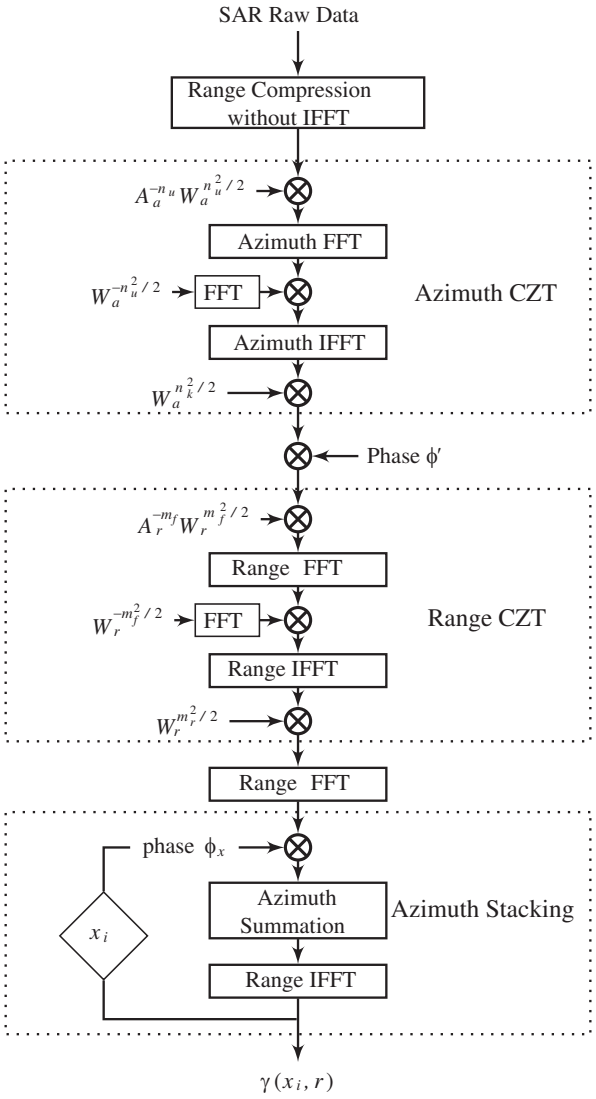

Figure 2. Block diagram of the proposed azimuth stacking algorithm via CZT processing. The algorithm can be divided into three parts: azimuth CZT, range CZT and azimuth stacking, as highlighted with dashed boxes.

3.1. Doppler Domain Mapping by CZT

Consulting (1), (2) and (4), we can find that the Doppler mapping can be done by the following scale Fourier transform,

$$S(\omega, k'_u) = \int S(\omega, u) \exp\left\{ - j\,\pi\, k'_u \frac{1}{\alpha(k)} u \right\} du. \tag{15}$$

According to the CZT algorithm [20], the mapped Doppler spectrum $S(\omega, k'_u)$ can be obtained by the following convolution and multiplication expressed in a discrete form as:

$$S(\omega, n_k) = \left\{ \left[S(\omega, n_u)\, A_a^{-n_u} W_a^{n_u^2/2} \right] \otimes W_a^{-n_u^2/2} \right\} \cdot W_a^{n_k^2/2}, \tag{16}$$

where $S(\omega, n_k)$ is the discrete form of $S(\omega, k'_u)$, with $n_k = 0, 1, \ldots, N_k - 1$; $S(\omega, n_u)$ is the discrete form of $S(\omega, u)$, with $n_u = 0, 1, \ldots, N_u - 1$; N_k and N_u are the number of samples in azimuth frequency domain and azimuth time domain, respectively. And $\otimes$ denotes the convolution which can be efficiently implemented with FFTs, and A_a and W_a are the factors defining the starting point and the angular spacing of the transform, respectively, and given as

$$A_a = \exp\left\{ -j\pi \frac{1}{\alpha(k)} \right\}, \tag{17}$$

$$W_a = \exp\left\{ -j \frac{2\pi}{N_k} \frac{1}{\alpha(k)} \right\}. \tag{18}$$

It should be noted that the above definitions of A_a and W_a mean that the CZT is evaluated on a part of the unite circle in the z-plane starting at the point A_a (negative frequency) and rotating counter-clockwise with spacing ratio defined by W_a [20]. This definition of the contour is appropriate for SAR processing, for we usually assume that the zero frequency of the signal is located at the center. Otherwise, such as defining the starting point at zero frequency point ($A_a = 1$), the CZT will lead to an undesired result due to the over scaling of the negative part of the frequencies. The implementation of (16) is illustrated as the first dotted part in the flow chart Fig. 2.

3.2. The Frequency Domain Mapping by CZT

Similarly, consulting (4), (6) and (7), the frequency domain mapping is equivalent to the following scaled inverse Fourier transform plus a range FFT,

$$S(r, k'_u) = \int S'(\omega, k'_u) \exp\left\{ j\pi 2k\, \beta(k'_u)\, r \right\} d(2k), \tag{19}$$

where

$$S'(\omega, k'_u) = S(\omega, k'_u) \cdot \underbrace{\exp\left\{ j2k \sqrt{1 - \left(\frac{k'_u}{2k_c} \right)^2}\, R_{tc} \right\}}_{\text{Phase } \phi'}.$$

R_{tc} denotes the center of the interesting range area, and phase ϕ' is used to take account the range offset [17].

According to the CZT algorithm, Equation (19) can be implemented via the following convolution and phase multiplication expressed in a discrete form

$$S(m_r, k'_u) = \left\{ \left[S'(m_f, k'_u)\, A_r^{-m_f} W_r^{m_f^2/2} \right] \otimes W_r^{-m_f^2/2} \right\} \cdot W_r^{\frac{m_r^2}{2}}, \tag{20}$$

where, $S(m_r, k'_u)$ is the discrete form of $S(r, k'_u)$, with $m_r = 0, 1, \ldots, M_r - 1$; $S'(m_f, k'_u)$ is the discrete form of $S'(\omega, k'_u)$, with $m_f = 0, 1, \ldots, M_f - 1$; M_r and M_f are the number of the samples in range time domain and range frequency domain, respectively. And $\otimes$ denotes the convolution which can be efficiently implemented with FFTs, and A_r and W_r are the factors defining the starting point and the angular spacing of the transform, respectively.

It is worth pointing out that by appropriately selecting R_{tc}, M_r and A_r, we can easily choose the sub-area to be imaged in the range domain. The sub-area processing can greatly reduce the time required in the stage of azimuth stacking. Supposing that the interesting range is $[R_{tc} - R_0, R_{tc} + R_0]$, where R_0 is the half width of the region. Then the range frequency CZT can be defined by the following steps:

- Phase ϕ multiplication;
- Calculating the range bin numbers;

$$M_r = 2\left\lceil \frac{R_0}{\triangle r} \right\rceil, \tag{21}$$

  where, $\lceil a \rceil$ denotes the smallest integer which is larger than a. $\triangle r = c\triangle t/2$ is the range bin size;
- Defining the angular spacing of the transform, W_r;

$$W_r = \exp\left\{ j\,\frac{2\pi}{M_k}\,\beta(k'_u) \right\}. \tag{22}$$

- Defining the starting point of the transform, A_r;

$$A_r = \exp\left\{ j\,\frac{2\pi}{M_k}\,\frac{M_r}{2}\,\beta(k'_u) \right\}. \tag{23}$$

The CZT based implementation of the frequency domain mapping, in the whole algorithm, has been diagrammatically shown in Fig. 2 as the dotted part of Range CZT. The mapped frequency domain data can be finally obtained by a range FFT of $S(r, k'_u)$.

3.3. Azimuth Stacking

The azimuth stacking processing has been explicitly summarized in Section 2.4, so will not be repeated here. The azimuth bins can be defined by the following steps assuming the azimuth region of interest is $2X_0$ with center X_c.

- Calculating the azimuth target bandwidth B_x using (9), as

$$B_x = \max\left[k_r \frac{k'_u}{\sqrt{4k_c^2 - {k'_u}^2}} \right] - \min\left[k_r \frac{k'_u}{\sqrt{4k_c^2 - {k'_u}^2}} \right]. \tag{24}$$

- Calculating the azimuth bin size

$$\triangle x = \frac{2\pi}{B_x}. \tag{25}$$

- then the azimuth bins x_i can be given as

$$N_x = 2\left\lceil \frac{X_0}{\triangle x} \right\rceil, \tag{26}$$

$$x_{i=1,\ldots,N_x} = \left[-\frac{N_x}{2}, \ldots, \frac{N_x}{2} - 1 \right] \triangle x + X_c. \tag{27}$$

4. COMMENTS ON THE NEW ALGORITHM

From the derivations, we can find that the proposed azimuth stacking algorithm is free of approximations. Thus, it should be an accuracy-optimal imaging method and can process SAR data regardless of the bandwidth, beamwidth and squint angle used. The proposed algorithm therefore can be served as a potential alternative to SAR image formation when the RD algorithms are invalid. In the processing, the CZT can be used to efficiently perform the two consecutive linear mappings that the reconstructed image does not suffer from interpolation truncation errors which usually accompanied with RMA algorithms.

However, due to its stacking property, the azimuth stacking algorithm is usually more time-consuming than other frequency domain methods (such as RD algorithms and RMA). For example, supposing there are M bins along Doppler domain and N bins along frequency domain for the 2D spectrum, and the image to be formed of size $m \times N$, then the number of computational operations of the proposed algorithm (based on CZT processing) can be roughly counted by: complex multiplications:

$4MN+MN\log_2(MN)+3MN\log_2(4MN)+mMN$ and complex additions: $2MN\log_2(4MN)+mMN$. Nevertheless, the azimuth stacking algorithm can form SAR image along each azimuth position without DFT wrap around errors [2]. Hence, a parallel computing architecture can be built to speed up the processing. Like other frequency domain methods, the azimuth stacking algorithm is vulnerable to motion errors. An effective motion compensation method for the new algorithm needs to be investigated in future.

5. SIMULATION RESULTS AND EXPERIMENTAL DATA EXAMPLES

In this section, the simulated and experimental data are used to validate the proposed azimuth stacking algorithm.

5.1. Results from Simulation Data

The point target simulation is employed to validate the proposed algorithm. In order to test the algorithm in a more generic way, the key parameters of the low frequency, ultra-wideband/widebeam (UWB/WB) P3 SAR system [22–24] has been adopted into the simulation case, as listed in Table 1. The severe range migration associated with the fine resolution UWB/WB SAR systems has been posing a significant challenge for most of the image formation algorithms [25]. In the simulation, 8 point targets have been placed uniformly around a circle of radius 80 m. Its center, with another point target assigned, is located at center range (500 m). This configuration of targets aims to validate the proposed algorithm's ability for image formation in all directions. Rectangular (uniform) window function is used for final reconstruction, for the sake of keeping the performance of the proposed algorithm.

Table 1. Parameters for the simulation.

Transmitted bandwidth	500 MHz
Carrier frequency	470 MHz
Waveform	Linear FM
Center squint angle	90 deg (broadside)
Effective beamwidth	50 deg
Center range	500 m
Range width	200 m
Azimuth width	200 m

In the simulation, the nonlinear Chirp scaling (NCS) method [11] is also implemented and compared with to better evaluate the performance of the proposed azimuth stacking algorithm (ASA). As a typical RD algorithm, the NCS method has being often used for SAR imaging in favor of its accuracy and efficiency. The simulation result is shown in Fig. 3, where Fig. 3(a) and Fig. 3(c) present the reconstructed point targets by ASA and NCS, respectively. Both of the images are plotted to -30 dB for a better displaying effect. The 2D contour plots of the impulse response function (IRF) of the right-most target (the squared point) are respectively shown in Fig. 3(b) and Fig. 3(d), after eight times interpolated along both azimuth and range domains. From Fig. 3(a) and Fig. 3(b), we can see that all the targets can be reconstructed quite well by the proposed algorithm. We can also notice the highly non-orthogonal sidelobes of the IRF, which is one of the characteristics of UWB/WB SAR systems. This kind of IRF of UWB SAR systems has been analysed in [26]. The non-rectangular spectrum poses challenges for conventional sidelobe reduction (apodization) techniques [27–29]. How to effectively suppress the non-orthogonal sidelobes still remains a problem. However, this beyonds the aim of the paper.

On the other hand, from Fig. 3(c) and Fig. 3(d), we can find that the targets are not reconstructed properly by the NCS method. This is not unexpected since the large fractional bandwidth and the wide antenna beamwidth used in the simulation makes the approximations of the RD algorithms (even with higher order) invalid. In order to further evaluate the focusing quantitatively, the typical image quality

parameters, including (−3 dB) Impulse Response Width (IRW), the Integrated Sidelobe Ratio (ISLR) and the Peak Sidelobe Ratio (PSLR), are also calculated and given in Table 2, where IRW_A(m) and IRW_R(m) denotes the IRW along azimuth and range directions, respectively. Considering the non-orthogonal sidelobes of the IRF, these parameters are obtained according to [30]. The processing times for the two methods are also listed in Table 2. From the above simulation results, we can see that the proposed ASA, comparing to the NCS, requires more processing time. This is mainly due to its inefficient stacking processing. However, an excellent image focus can be achieved by the proposed algorithm, which is an accuracy-optimal imaging method and can process SAR data regardless of the bandwidth, beamwidth and squint angle used.

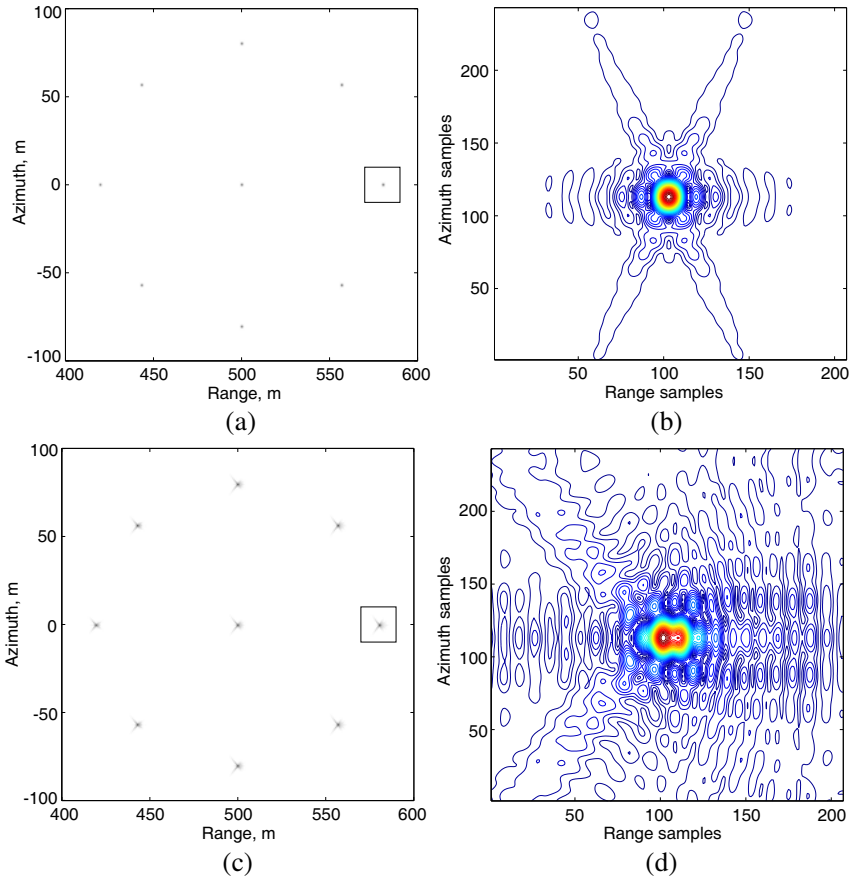

Figure 3. Point target simulation results: (a) and (c) show the reconstructed images by the proposed azimuth stacking algorithm (ASA) and the nonlinear Chirp scaling (NCS) algorithm, respectively. Both of the reconstructed images are plotted to −30 dB for a better displaying effect. And the 2D contour plots of the IRF for the right-most target (the squared point in the reconstructed image) are displayed in (b) and (c) correspondingly, after eight times interpolated along both azimuth and range domains. (a) The reconstructed image (ASA). (b) The IRF contour plots (ASA). (c) The reconstructed image (NCS). (d) The IRF contour plots (NCS).

Table 2. Processing times and image quality parameters of the simulation.

Method	Tim(s)	IRW_A(m)	IRW_R(m)	ISLR(dB)	(dB)
ASA	180.5	0.58	0.56	−5.27	−12.26
NCS	16.7	0.72	0.86	−1.22	−9.17

5.2. Results from Experimental Data

The experimental UWB SAR raw data are collected in an anechoic chamber. A pair of Archimedean spiral antennas (mutual distance: 0.79 m) is used to transmit and receive radar signals as depicted in Fig. 4(a). The antennas are placed on an movable equipment, which can be accurately controlled by the software, to form the synthetic aperture. A network analyzer (Agilent N5242A) is used to generate the stepped-frequency signal covering a bandwidth from 0.5 to 2.5 GHz, with a step size of 1 MHz. The targets consists of two dihedral reflectors (T1, T2), two trihedral reflectors (T3, T4), and a metallic sphere (T5), as shown in Fig. 4(b). The specific geometry of the imaging scene is depicted in Fig. 4(c). The image produced by the proposed azimuth stacking algorithm is displayed in Fig. 4(d). Comparing Fig. 4(c) and Fig. 4(d), we can find that all targets can be very well reconstructed by the proposed algorithm.

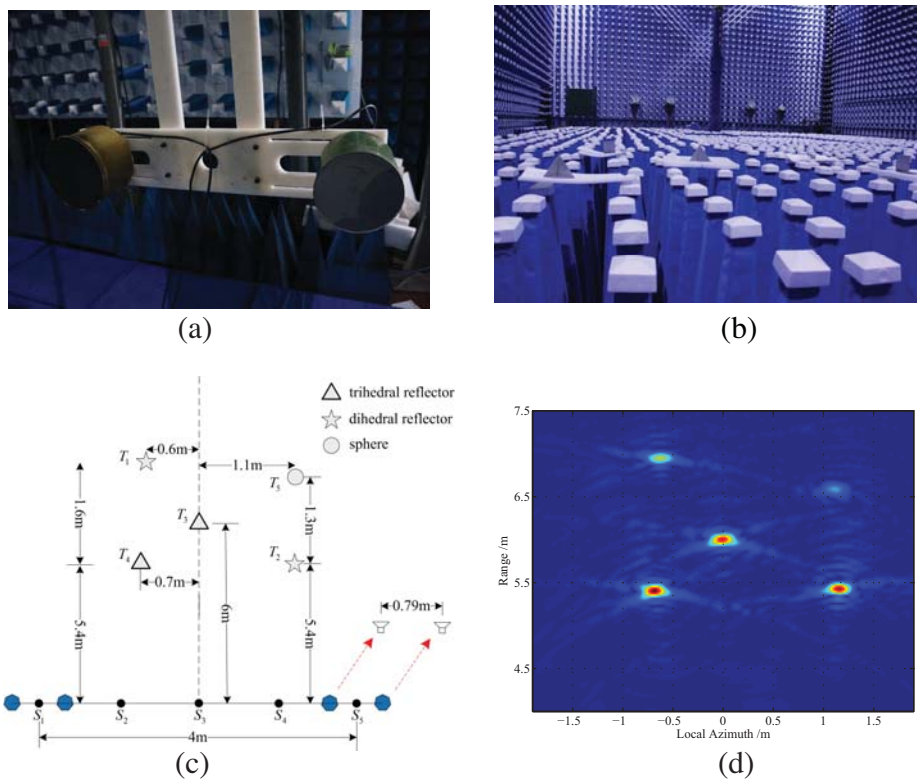

Figure 4. The experimental measurement setup and the imaging result. (a) Archimedean spiral antennas working as tansmitter (right) and receiver (left). (b) Photo of the five targets. (c) Specific geometry of the imaging scene. (d) Imaging result.

6. CONCLUSIONS

We propose a new frequency domain SAR imaging method: azimuth stacking algorithm. After two consecutive linear mappings along Doppler and frequency domains, the original range-dependent SAR transfer function becomes into azimuth-dependent. Then, SAR image can be reconstructed by the stacking method along azimuth direction. The algorithm can form SAR image at each azimuth position without DFT wrap around errors. Interpolation can also be avoided in the reconstruction if Chirp z-transform (CZT) is used to perform the two consecutive linear mappings. Finally, the effectiveness of the proposed algorithm have been validated by both the numerical simulations and the experimental measurements.

ACKNOWLEDGMENT

This work was supported by the National Basic Research Program of China under Grant 2010CB951403 and the National Natural Science Foundation of China under Grants 41071227, 91025001, and 61271441.

REFERENCES

1. Curlander, J. C. and R. N. McDonough, *Synthetic Aperture Radar: Systems and Signal Processing*, Wiley, New York, 1991.
2. Soumek, M., *Synthetic Aperture Radar Signal Processing with MATLAB Algorithms*, Wiley, New York and N.Y. [etc.], 1999.
3. Frey, O., C. Magnard, M. Ruegg, and E. Meier, "Focusing of airborne synthetic aperture radar data from highly nonlinear flight tracks," *IEEE Transactions on Geoscience and Remote Sensing*, Vol. 47, No. 6, 1844–1858, 2009.
4. Yegulalp, A. F., "Fast backprojection algorithm for synthetic aperture radar," *Proc. Record of the 1999 IEEE Radar Conf.*, 60–65, 1999.
5. Ulander, L. M. H., H. Hellsten, and G. Stenstrom, "Synthetic-aperture radar processing using fast factorized back-projection," *IEEE Transactions on Aerospace and Electronic Systems*, Vol. 39, No. 3, 760–776, 2003.
6. Frolind, P.-O. and L. M. H. Ulander, "Evaluation of angular interpolation kernels in fast back-projection SAR processing," *IEE Proceedings — Radar, Sonar and Navigation*, Vol. 153, No. 3, 243–249, 2006.
7. Demanet, L., M. Ferrara, N. Maxwell, J. Poulson, and L. Ying, "A butterfly algorithm for synthetic aperture radar imaging," *SIAM J. Img. Sci.*, Vol. 5, 203–243, Feb. 2012.
8. Cumming, I. G. and F. H. Wong, *Digital Processing of Synthetic Aperture Radar Data: Algorithms and Implementation*, Artech House, Boston, 2005.
9. Runge, H. and R. Bamler, "A novel high precision SAR focussing algorithm based on chirp scaling," *Proc. Int. Geoscience and Remote Sensing Symp. IGARSS'92*, 372–375, 1992.
10. Raney, R. K., H. Runge, R. Bamler, I. G. Cumming, and F. H. Wong, "Precision SAR processing using chirp scaling," *IEEE Transactions on Geoscience and Remote Sensing*, Vol. 32, No. 4, 786–799, 1994.
11. Davidson, G. W., I. G. Cumming, and M. R. Ito, "A chirp scaling approach for processing squint mode SAR data," *IEEE Transactions on Aerospace and Electronic Systems*, Vol. 32, No. 1, 121–133, 1996.
12. Moreira, A. and Y. Huang, "Airborne SAR processing of highly squinted data using a chirp scaling approach with integrated motion compensation," *IEEE Transactions on Geoscience and Remote Sensing*, Vol. 32, No. 5, 1029–1040, 1994.
13. Moreira, A., J. Mittermayer, and R. Scheiber, "Extended chirp scaling algorithm for air- and spaceborne SAR data processing in stripmap and scansar imaging modes," *IEEE Transactions on Geoscience and Remote Sensing*, Vol. 34, No. 5, 1123–1136, 1996.
14. Wang, K. and X. Liu, "Quartic-phase algorithm for highly squinted SAR data processing," *IEEE Geoscience and Remote Sensing Letters*, Vol. 4, No. 2, 246–250, 2007.
15. Zaugg, E. C. and D. G. Long, "Generalized frequency-domain SAR processing," *IEEE Transactions on Geoscience and Remote Sensing*, Vol. 47, No. 11, 3761–3773, 2009.
16. Cafforio, C., C. Prati, and F. Rocca, "SAR data focusing using seismic migration techniques," *IEEE Transactions on Aerospace and Electronic Systems*, Vol. 27, No. 2, 194–207, 1991.
17. Bamler, R., "A comparison of range-Doppler and wavenumber domain SAR focusing algorithms," *IEEE Transactions on Geoscience and Remote Sensing*, Vol. 30, No. 4, 706–713, 1992.
18. Zhe, L., W. Jian, and L. Q. Huo, "Interpolation-free Stolt mapping for SAR imaging," *IEEE Geoscience and Remote Sensing Letters*, Vol. 11, No. 5, 926–929, 2014.

19. Reigber, A., E. Alivizatos, A. Potsis, and A. Moreira, "Extended wavenumber-domain synthetic aperture radar focusing with integrated motion compensation," *IEE Proceedings — Radar, Sonar and Navigation*, Vol. 153, No. 3, 301–310, 2006.
20. Rabiner, L., R. Schafer, and C. Rader, "The chirp z-transform algorithm," *IEEE Transactions on Audio and Electroacoustics*, Vol. 17, No. 2, 86–92, 1969.
21. Lanari, R., "A new method for the compensation of the SAR range cell migration based on the chirp z-transform," *IEEE Transactions on Geoscience and Remote Sensing*, Vol. 33, No. 5, 1296–1299, 1995.
22. Sheen, D. R., C. M. Strawitch, and T. B. Lewis, "UHF wideband SAR design and preliminary results," *Proc. Int. Geoscience and Remote Sensing Symp. IGARSS'94. Surface and Atmospheric Remote Sensing: Technologies, Data Analysis and Interpretation*, Vol. 1, 289–291, 1994.
23. Sheen, D. R., S. J. Shackman, N. L. VandenBerg, D. L. Wiseman, L. P. Elenbogen, and R. F. reRawson, "The p-3 ultra-wideband SAR: description and examples," *Proc. IEEE National Radar Conf.*, 50–53, 1996.
24. Soumekh, M., D. A. Nobles, M. C. Wicks, and G. R. J. Genello, "Signal processing of wide bandwidth and wide beamwidth p-3 SAR data," *IEEE Transactions on Aerospace and Electronic Systems,*, Vol. 37, No. 4, 1122–1141, 2001.
25. Goodman, R., S. Tummala, and W. Carrara, "Issues in ultra-wideband, widebeam SAR image formation," *Proc. Record of the IEEE 1995 Int. Radar Conf.*, 479–485, 1995.
26. Vu, V. T., T. K. Sjogren, M. I. Pettersson, and H. Hellsten, "An impulse response function for evaluation of UWB SAR imaging," *IEEE Transactions on Signal Processing*, Vol. 58, No. 7, 3927–3932, 2010.
27. DeGraaf, S. R., "SAR imaging via modern 2-D spectral estimation methods," *IEEE Transactions on Image Processing*, Vol. 7, No. 5, 729–761, 1998.
28. Stankwitz, H. C., R. J. Dallaire, and J. R. Fienup, "Nonlinear apodization for sidelobe control in SAR imagery," *IEEE Transactions on Aerospace and Electronic Systems*, Vol. 31, No. 1, 267–279, 1995.
29. Harris, F. J., "On the use of windows for harmonic analysis with the discrete Fourier transform," *Proceedings of the IEEE*, Vol. 66, No. 1, 51–83, 1978.
30. Vu, V. T., T. K. Sjogren, M. I. Pettersson, and A. Gustavsson, *Definition on SAR image quality measurements for UWB SAR*, 71091A–71091A–9, SPIE — International Society for Optical Engineering, Oct. 2008.